Experimental Study on the Effect of Realistic Shapes on Single-Grain Crushing Characteristics of Fragmented Weathered Phyllite as Subgrade Filler

Yanjie Zhang[1], Gong Liu[1], Xu Wang[2], Hanxing Zhu[3], Liang An[4]

[1] School of Civil Engineering， Lanzhou Jiaotong University, Lanzhou 730070, China

[2] National and Provincial Joint Laboratory of Road & Bridge Disaster Prevention and Control, Lanzhou Jiatong University, Lanzhou 730070, China

[3] School of Engineering, Cardiff University, Cardiff CF24 3AA, UK

[4] College of Earth and Environmental Science, Lanzhou Jiaotong University, Lanzhou 730070, China

Abstract

Grain morphology—a fundamental characteristic of granular materials—significantly influences their macroscopic behavior. This study comprehensively investigates the effect of crushing strength distribution, crushing mode, force–displacement curve, size, and realistic shape characteristics on the crushing behavior of weathered phyllite grains. A series of single-particle crushing tests was conducted to examine the Weibull distribution and crushing strength of weathered phyllite grains; three representative grain morphologies were considered: general form, local roundness, and surface roughness. Realistic shape characteristic parameters before and after particle crushing were obtained using three-dimensional scanning and image processing techniques. The results demonstrate that the particle crushing strength distribution of weathered phyllite grains can be accurately described using a Weibull function. The Weibull modulus, characteristic strength, and crushing strength of the weathered phyllite grains decreased with increasing grain size. Moreover, the three fragmentation modes—fracturing, splitting, and chipping—corresponded to the force–displacement curves displaying single-peak, double-peak, and multipeak characteristics, respectively. Furthermore, flatter and more slender grains exhibited more prominent angular characteristics. While smoother grain surfaces were more susceptible to fracture failures, rougher surfaces were less prone to such failures. These findings demonstrate the pronounced size effect observed in weathered phyllite grains. Furthermore, compared to the original weathered phyllite grains, an increase in fineness, angularity, and surface roughness, along with a decrease in flatness, was observed in the subparticles resulting from crushing. These findings provide a theoretical reference for the engineering application of weathered phyllite as roadbed filler material in mountainous projects and deeper insights into the effect of morphological features on grain crushing behaviors.

Introduction

Granular materials comprise interconnected solid particles (Deresiewicz 1958). They are prevalent in nature and daily life, and extensively used in hydraulic engineering, civil engineering, transportation, mineralogy, chemical engineering, and pharmaceutical engineering. In geotechnical engineering, granular materials (e.g., mineral grains, sedimentary deposits, and rock masses) exhibit exceptional engineering characteristics, which include high packing density, excellent compaction performance, strong permeability to water flow, and high shear strength.

They also resist deformation under a load with minimal settlement. Moreover, owing to their wide distribution range and high bearing capacity, they are widely employed in applications, such as the construction of rockfill dams (Jin et al. 2024; Marachi 1969; Wei et al. 2010), highway and railway embankments (McKenna et al. 2021; Miščević and Vlastelica 2019; Riviera et al. 2014; Wang et al. 2022a, b, 2024; Wen et al. 2025; Wu 2004), railway ballast (Kashani et al. 2017; Zheng et al. 2022), and backfilling in coal mining operations (Le et al. 2021; Li et al. 2019).

The construction of several interconnecting highways and railways in the mountainous regions of western China has resulted in an increased number of tunnels and road cuttings owing to the geological disparities in these regions. Significant variations in the terrain height necessitate numerous deep excavations and long tunnels, leading to a substantial amount of waste material. Additionally, there is a shortage of high-quality fillers, which further escalates the cost of subgrade fillers because of their long-distance transportation and high unit prices (Mao et al. 2017; Zhang et al. 2014). Consequently, road construction faces challenges, such as insufficient roadbed fillers and excessive excavation materials. To align with the new construction concepts of conservation, environmental protection, and sustainability, as well as to meet the linear requirements of road design, it is appropriate to implement a balanced approach to filling and excavation. By effectively utilizing waste materials (Feng et al. 2024; Liu et al. 2020), the problem of roadbed fillers can be efficiently addressed during road construction.

Phyllite is a low-grade metamorphic rock exhibiting an intermediate degree of metamorphism between slate and schist, characterized by its phyllitic structure (Garzón et al. 2015). Owing to artificial blasting, mining, and other factors, the phyllite waste grains contain numerous defects such as micropores and microcracks as well as possessing irregular shapes with distinct angular characteristics. Consequently, when using phyllite particles as embankment-filling materials during compaction processes, significant particle crushing occurs under the influence of rolling, tamping, and vibration. Particle crushing leads to increased compressibility and reduced strength of the material, resulting in substantial deformation that ultimately causes overall instability and failure of the geostructure (Xiao et al. 2020b; Zhou et al. 2019).

Grain breakage is a crucial characteristic of granular materials and has been the focus of numerous studies in recent decades (Huang et al. 2020; McDowell and Harireche 2002; Werkmeister et al. 2005; Xiao et al. 2020a). It significantly influences the macromechanical behavior of granular materials. At the mesolevel, grain breakage alters particle contact relationships and induces reorganization within the mesostructure, thereby impacting its evolution. On the macroscale, grain breakage directly affects particle material gradation, which plays an important role in determining the strength characteristics, dilatancy, internal friction angle, porosity, pore-water pressure, and permeability coefficient of particle materials (Bolton et al. 2008; Li et al. 2023; Necochea et al. 2024).

The characterization of single-grain breakage serves as the foundation for analyzing the fracture characteristics within particle systems. Conducting a single-particle crushing test allows for the easy observation of particle fragmentation and accurate acquisition of information regarding particle crushing. Currently, most single-particle compression tests focus on rock and sand particles, primarily investigating parameters such as the crushing strength, mode of failure, force–displacement curve characteristics, and distribution of the crushing strength (McDowell and Bolton 1998; Sefi and Lav 2022; Zhou et al. 2020). An increasing number of researchers have examined the influence of grain shape on the mechanical behavior of granular materials (Huang et al. 2023; Koutous and Hilali 2019; Xiao et al. 2019; Zhao et al. 2021b; Zhou et al. 2013). Consequently, consideration of realistic grain shapes when studying grain breakage has become a prominent topic. Recent studies indicate that the grain shape significantly impacts the fracture

patterns and crushing strength of the grains (Ma et al. 2017; Neveu et al. 2016; Shi et al. 2021; Ying et al. 2021).

Over the past two decades, various measurement techniques have been employed to acquire the morphologies of individual grains, including conveyors equipped with multiple cameras (Maerz and Luscher 2001), stereo photography systems (Zheng and Hryciw 2017), three-dimensional (3D) laser scanning techniques (Hayakawa and Oguchi 2005; Huang et al. 2020; Illerstrom 1998; Lanaro and Tolppanen 2002; Latham et al. 2008; Ouhbi et al. 2017; Sun et al. 2014; Xie et al. 2020), and X-ray computed tomography (CT) (Wu and Wang 2024; Zheng et al. 2020). The 3D laser scanning technique was initially applied to investigate ballast materials by Illerstrom (1998). Lanaro and Tolppanen (2002) devised a novel method for characterizing the dimensions, shape, and roughness of aggregate particles based on 3D laser scanning and evaluation of the coarse-grained aggregate particle images. Subsequently, researchers employed 3D laser scanning techniques to acquire precise size and shape characterizations of various materials, including gravel (Hayakawa and Oguchi 2005), rock aggregate (Latham et al. 2008), ballast (Ouhbi et al. 2017; Sun et al. 2014), natural sand (Xie et al. 2020), and pebble (Huang et al. 2020). This high-resolution 3D surface morphology analysis enabled the measurement of grain properties such as volume, surface area, and three Feret diameters in 3D space (Ouhbi et al. 2017). Hence, the suitability of the 3D laser scanning technique for capturing coarse aggregate-sized grains (10–100 mm) was confirmed.

The significance of single-particle failure on the mechanical properties and deformation characteristics of granular materials has been acknowledged in previous studies. Single-particle compression tests using two polished rigid plates are commonly employed to investigate grain breakage behavior (McDowell and Bolton 1998; Wang and Coop 2016; Yin et al. 2023). Previous experimental findings have demonstrated that factors such as grain size, angularity, mineralogy, and single-grain tensile strength influence the compression behavior of granular materials (Meng et al. 2022a; Nakata et al. 2001; Wang and Coop 2016; Yin et al. 2023). Nakata et al. (2001) proposed the following five modes of grain crushing in one-dimensional compression tests: no visible damage, single abrasion, multiple asperity fractures, major splitting, and further crushing of subparticles. Moreover, it has been theoretically and experimentally demonstrated that the strength of grain crushing follows a Weibull distribution (McDowell and Amon 2000; Meng et al. 2022a; Weibull 1951). Weibull survival probability plots were generated to investigate the statistical characteristics of the crushing strengths of the tested particles. However, there is still a limited consensus on grain breakage criteria, and the mechanisms underlying breakage remain uncertain (Meng et al. 2022a).

Despite recent advancements, previous studies have predominantly focused on natural granular materials such as gravel, pebbles, sand, and ballast. However, limited research has been conducted on the weathered phyllite resulting from artificial excavation or blasting. Furthermore, few studies have considered the particle morphology when investigating the crushing strength and related statistics of individual particles. Consequently, a comprehensive understanding of the crushing characteristics of weathered phyllite grains is required. To address these limitations, this study presents a single-particle compression test that examines weathered phyllite with varying particle sizes and shapes. The crushing strength distribution, crushing mode, form of the force–displacement curve, and size effect of the weathered phyllite grains were analyzed. In addition, the particle crushing strength was evaluated using the Weibull statistical model. Additionally, 3D-scanning and image processing techniques were employed to obtain the characteristic shape parameters of the weathered phyllite grains before and after crushing. Subsequently, the influence of a realistic shape on the crushing mode was examined, and the variation in the grain shape characteristics before and after crushing was analyzed.

Materials and Methods

Basic Properties of Weathered Phyllite

Weathered phyllite grains were collected from a highway construction project in the Longnan Area of Gansu Province, China (Fig. 1). The crushed weathered phyllite grains exhibited a flake-like and fragmented morphology with an uneven particle-size distribution.

Fig. 1. Weathered phyllite filler studied.

X-ray powder diffraction (XRD) analysis was conducted to determine the mineralogy of the weathered phyllite, and the results are presented in Fig. 2. The mineral composition of the weathered phyllite was characterized by significant proportions of muscovite (38.0%), orthoclase (27.1%), kaolinite (22.5%), and quartz (12.4%). Notably, compared to the phyllites found in other regions, the weathered phyllite exhibited elevated concentrations of muscovite as well as orthoclase, and relatively lower levels of quartz (Garzón et al. 2010; Li et al. 2024; Liu et al. 2020; Zhao et al. 2021c).

The chemical composition of the sample, as determined via X-ray fluorescence (XRF) analysis (Table 1), indicates the moisture content is 3%–6.7% and bulk density is 71–72.83 g/cm^3 of the phyllite slag excavated from the tunnel.

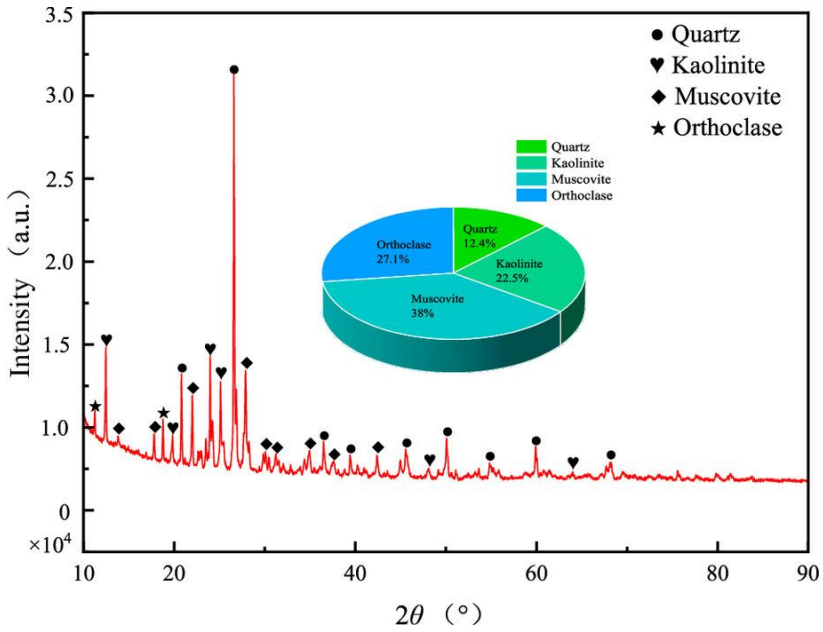

Fig. 2. XRD and XRF analyses of phyllite.

Table 1. Summary of chemical composition of the phyllite sample using XRF

Chemical composition	Content (%)
SiO_2	59.0
Al_2O_3	24.1
Fe_2O_3	4.85
K_2O	4.67
MgO	2.91
Na_2O	2.70

Point-load tests were performed on rock blocks composed of weathered phyllite using a point-load testing machine following the guidelines set by the International Society for Rock Mechanics (ISRM) (Franklin 1985). The point-load strength index was determined using the method described by Singh et al. (2012). The point-load strength index values ranged between 0.94 and 6 MPa for weathered phyllite, with an average value of 3.39 MPa. Consequently, based on its properties, the weathered phyllite block can be classified as a type of soft rock (Heidari et al. 2013; Liu et al. 2020; Mao et al. 2017).

Because of the diverse shapes of fragmented phyllite grains, relying solely on sieve analysis to determine particle size is not sufficiently reasonable. The maximum dimensions of the screened phyllite grains were measured using calipers as an indicator of grain size (Zheng et al. 2019). Subsequently, the sizes were categorized into the following three groups: 5–10, 10–20 and 20–31.5 mm (Fig. 3). Each group consisted of 100 particles.

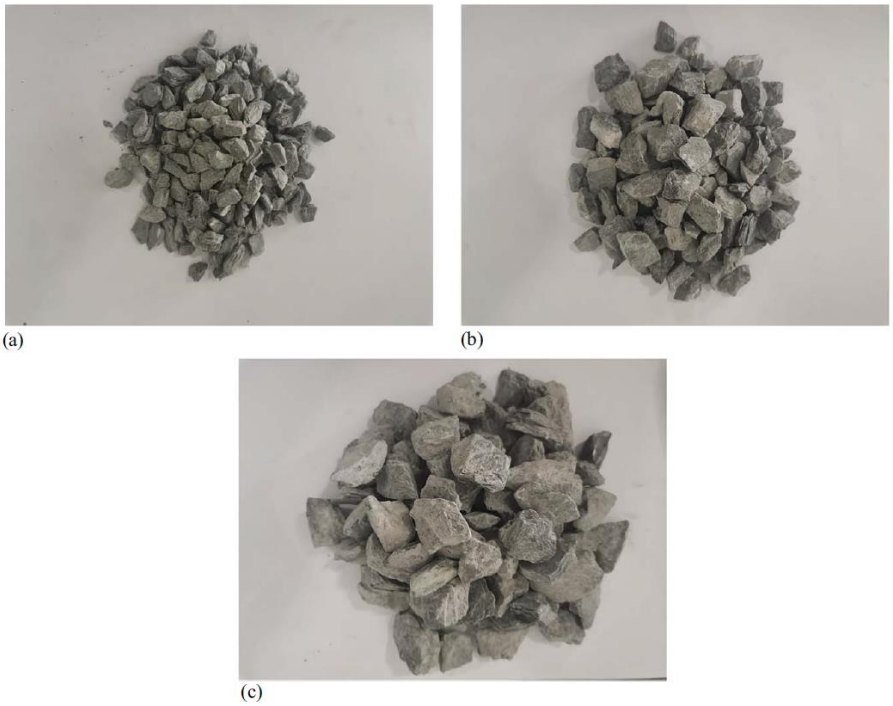

Fig. 3. Phyllite grains: (a) 5–10 mm; (b) 10–20 mm; and (c) 20–31.5 mm.

Grain Surface Geometry Acquisition

Grain morphologies were obtained using a 3D scanner, as shown in Fig. 4. This scanning technique closely resembled that employed by Huang et al. (2020). The entire scanning system comprised three components: the scanner host, an automatic turntable, and a computer. The structural light source captures the position coordinate data of the scanned object using a high-definition camera. The scanning system was equipped with four industrial-grade high-definition cameras offering a scanning accuracy range of 0.001–0.05 mm. The accuracy was sufficient for rock grains within the size range of 5–40 mm. Using an automatic turntable, an object can be scanned from eight angles, covering a complete 360-degree view. Additionally, to capture the comprehensive 3D morphology of each grain, manual rotation was required to scan both the top and bottom surfaces. Subsequently, the scanning data were transmitted to the computer's scanning software via a Universal Serial Bus (USB) transmission line and intelligently merged into a unified point-cloud layer. Using Geomagic Studio software, the scanning results from various angles were aligned and seamlessly combined, allowing for the rescanning of any missing parts.

A total of 300 weathered phyllite grains were selected, with 100 particles in each particle-size group. The 3D surface geometry acquisition process of the particles following the completion of scanning is illustrated in Fig. 5. The weathered phyllite grains were coated with an imaging agent and scanned using a 3D scanner to obtain point cloud data. The scanned images were then stitched and merged. The 3D point cloud data were gridded using the Flex Scan 3D software in the instrument and saved in STL format. After completing the initial scanning, the Geomagic Studio software used for processing the 3D models was employed to address any holes, nails, or suspended impurities that were not connected to the main body of the model. Finally, 3D shape images of the weathered phyllite particles were obtained.

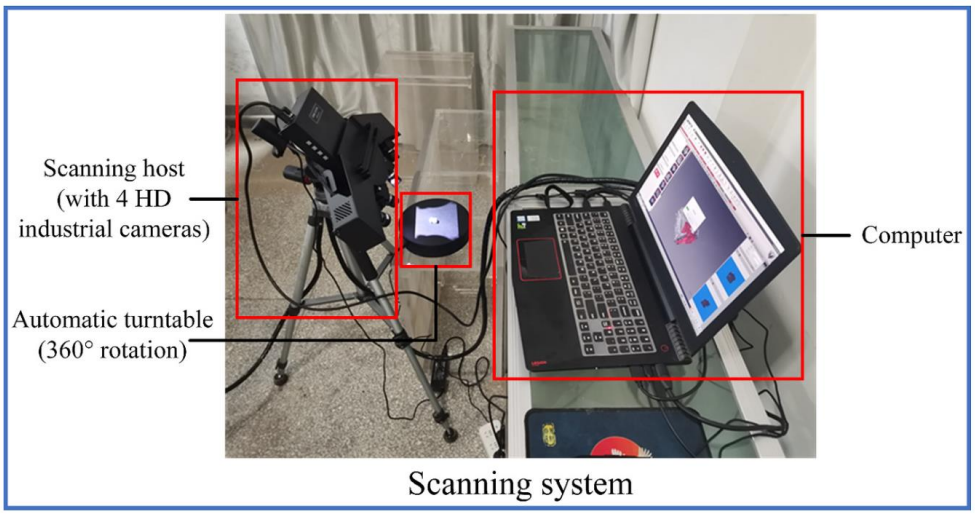

Fig. 4. 3D scanning system.

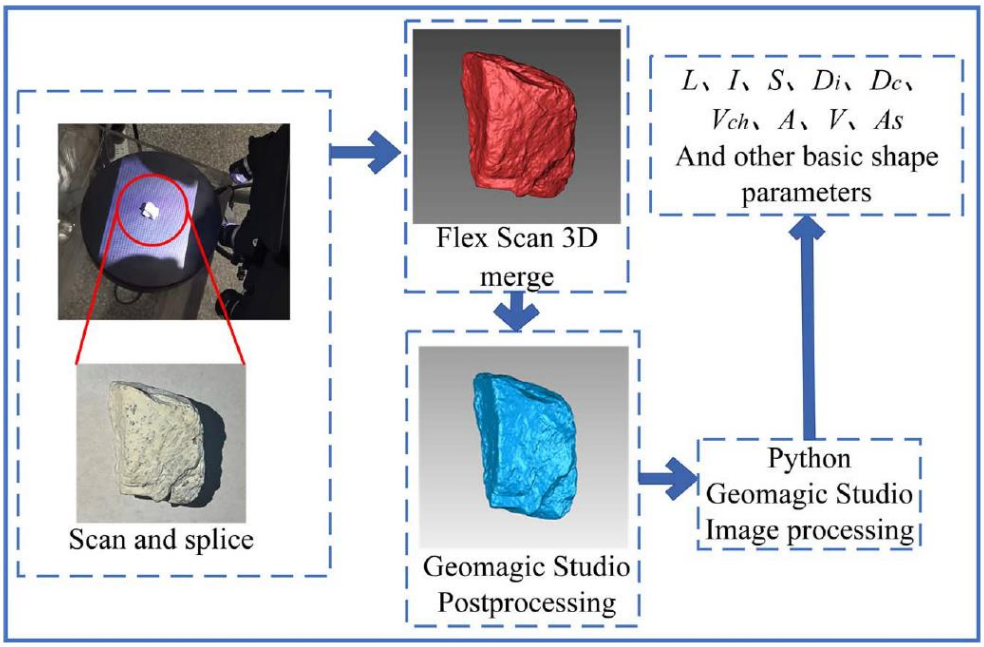

Fig. 5. 3D surface geometry acquisition process.

The generated surface mesh files were imported and processed using MeshLab 3D image processing software to generate an optimized mesh (Cignoni et al. 2008; Huang et al. 2020). The point-cloud data set obtained from the scanner was characterized by high density, which could result in an exceptionally refined finite-element mesh. Huang et al. (2020) concluded that when discretizing a rock grain surface with a minimum of 2,000 triangle elements, the roughness of the grain surface had minimal influence on the macroscopic response of granular soils. Therefore, we deemed it sufficient to select 50,000 triangular elements.

Quantitative analysis of the grain shape was conducted using various shape descriptors (Domokos et al. 2015; Garboczi et al. 2012; Huang et al. 2023; Ma et al. 2018; Maroof et al. 2020; Mollon and Zhao 2012; Pouranian et al. 2020; Zheng and Hryciw 2015; Zingg 1935). Python code was employed to extract the grain dimensions by constructing a bounding box around each grain. The relevant statistics include the long axis (L), intermediate axis (I), and short axis (S). In addition,

the surface area (A), volume (V), and convex-hull volume (V_{ch}) were calculated (Huang et al. 2023). A multiscale description of the grain morphology was developed at three levels (Liang et al. 2022; Wang et al. 2017): large-scale (general form), medium-scale (local roundness), and small-scale (surface roughness). The large-scale level corresponded to the overall shape of the particle, whereas the medium-scale level captured its surface edges and corners. The small-scale level provided details on the surface texture and roughness. The other shape parameters derived from the fundamental quantities are listed in Table 2.

Table 2. Shape descriptor of the grains

Type	Parameter	Formula
General form	Elongation ratio (Maroof et al. 2020; Zingg 1935)	$E_r = S/I$
	Flatness ratio (Maroof et al. 2020; Zingg 1935)	$F_r = I/L$
	Domokos shape factor (Domokos et al. 2015; Ma et al. 2018)	$S_f = \left(\frac{1}{S}+\frac{1}{I}+\frac{1}{L}\right)\sqrt{S^2+I^2+L^2}/\sqrt{3}$
Local roundness	True sphericity (Garboczi et al. 2012; Maroof et al. 2020)	$\psi_{3D} = \frac{A_S}{A} = \frac{\sqrt[3]{36\pi V^2}}{A}$
	Inscribed circle sphericity (Huang et al. 2023; Maroof et al. 2020)	$\phi_0 = \frac{D_i}{D_c}$
	Volume sphericity (Huang et al. 2023; Maroof et al. 2020)	$\phi_V = \frac{V_i}{V_c} = \left(\frac{D_i}{D_c}\right)^3$
Surface roughness	Convexity (Huang et al. 2023; Maroof et al. 2020)	$C_X = \frac{V}{V_{ch}}$
	Regularity (Mollon and Zhao 2012; Pouranian et al. 2020)	$R = \log\left(\frac{V}{V_{ch}-V}\right)$

Note: A_s = surface area of a sphere with same particle volume; D_i and V_i = diameter and volume of the maximum inscribed sphere; and D_c and V_c = diameter and volume of the minimum circumscribed sphere.

Grain Crushing Experimental Procedure

The electronic pressure testing machine (MTS CDT1305-2) was employed to conduct particle crushing tests, with a loading speed ranging from 0.01 to 50 mm/min and a testing range of 10–300 kN. The precision of the machine was 0.01 kN. The testing apparatus consisted of three components: a computer, a measurement and control system, and a host computer (Fig. 6). To ensure the most stable positioning of the grains on the bottom platen, the plane formed by the long (L) and intermediate (I) axes of the phyllite particles was aligned parallel to the plane of the loading platen. Adjustments were made by rotating the grains until their bottom region achieved a minimal distance, indicating a lower center of gravity (Huang et al. 2020, 2023). After preloading, the upper loading platen maintained a stable contact with the top surface of the grain. Subsequently, a lower-loading platen was used to apply a constant compression rate of 2 mm/min to the grains.

The test was considered complete when cracks penetrated or significant debris formation occurred, leading to destruction of the main body of the grains. The fragmented particles were carefully collected and assigned unique identification numbers for subsequent 3D scanning analysis, enabling the investigation of the shape variations of weathered phyllite particles before and after crushing.

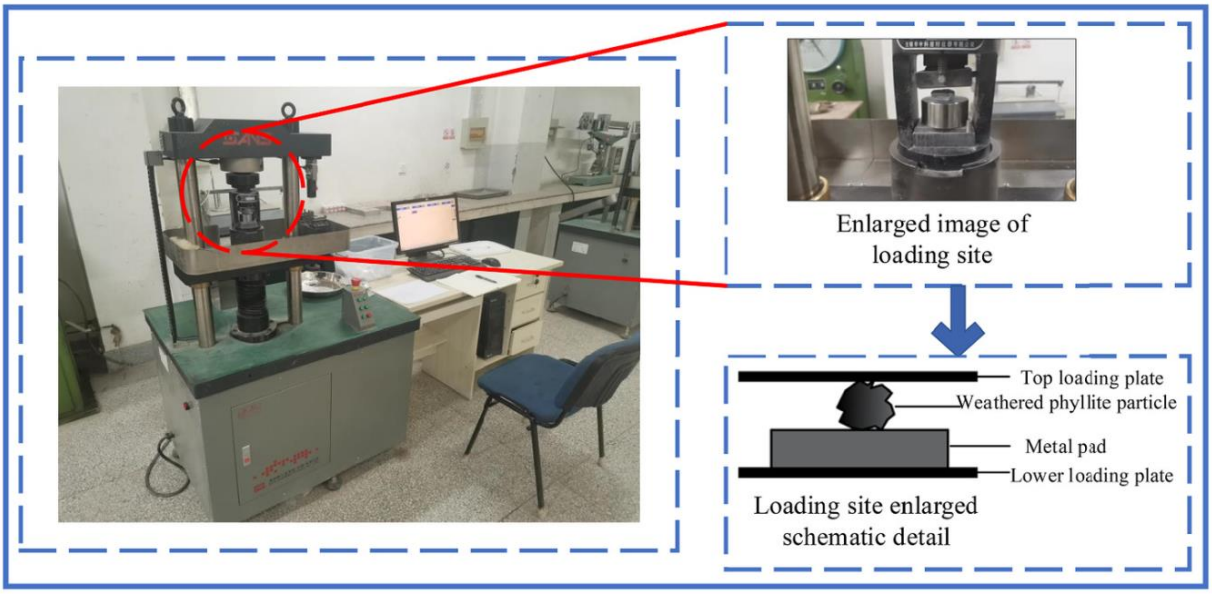

Fig. 6. Particle crushing apparatus and loading diagram.

Experimental Results

Load Characteristics and Crushing Mode

The displacement and force of the lower platen were recorded during the particle-crushing tests. A representative force–displacement curve is shown in Fig. 7. It can be inferred that the failure process can be categorized into the following three distinct stages: adjustment, elastic response, and crack propagation.

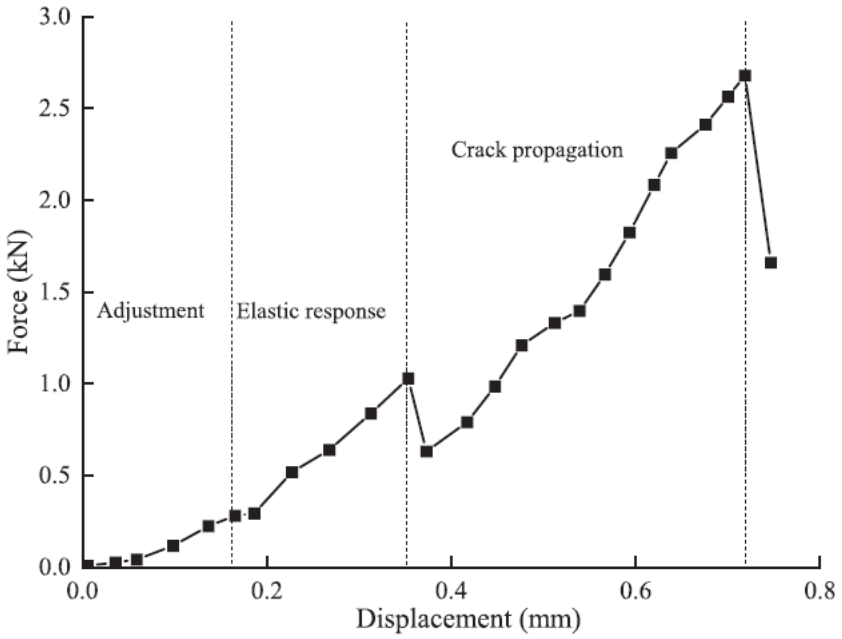

Fig. 7. Representative force–displacement curve.

During the adjustment stage, as the grains made contact with the upper loading platen, a relatively slow growth rate of the force on the phyllite grains was observed. At this stage, the particles do not attain a fully stable stress state because their convex edges are in contact with the curved surface formed by the loading plate. Subsequently, upon reaching a completely stable stress state, they transition into an elastic response stage characterized by a gradual increase in the force growth rate and a linear relationship between force and displacement. No cracks were observed on the grain surfaces. However, when the force exceeded a certain threshold, the edges and corners of the grains underwent fracturing, resulting in an initial decrease in force. With a further increase in force, the grains entered a stage of crack propagation, where internal cracks gradually extended outward under the influence of the applied force, eventually leading to visible surface cracks. Upon reaching the peak crushing point, the cracks expanded rapidly until they penetrated the entire grain structure. Subsequently, fractures occurred along these cracks, and the force rapidly decreased until complete failure was achieved. This observation aligns with previous findings by Nakata et al. (2001), Huang et al. (2020), and Wang et al. (2017).

Various crushing modes for single particles have been proposed in previous studies (Meng et al. 2022a; Wang and Coop 2016; Weibull 1951). Wang and Coop (2016) suggested that the fragmentation of a single grain can be categorized into the following five modes: (1) splitting, (2) explosive, (3) chipping, (4) mixed, and (5) core remaining. However, observing all the fragmentation modes in a single test is not possible. Typically, two or three fragmentation modes can be observed in one test (Meng et al. 2022a). In this study, based on the analysis of grain morphology and the number of peak force points, the fragmentation modes of weathered phyllite grains can be classified into three categories: fracturing, splitting, and chipping, as illustrated in Fig. 8. The force–displacement curves exhibited both single-peak and multipeak features. The proportions of these three fragmentation modes within each grain-size group are presented in Table 3.

1. Fracturing: As shown in Fig. 8(a), with an increasing force, the weathered phyllite grains instantaneously fractured from the middle and split into two grains along the fracture surface. The force–displacement curve exhibited a single peak, which initially displayed a smooth behavior. Upon reaching the crushing peak point, the curve sharply declined as the cracks rapidly propagated throughout the entire grain.

2. Splitting: As illustrated in Fig. 8(b), the expansion of cracks resulted in the splitting of weathered phyllite grains into three to five pieces along the fracture surface without generating numerous small fragments (Nakata et al. 2001). The force–displacement curve exhibited a double peak, with the second peak point being generally higher than the first. Upon reaching this second force peak point, the curve sharply decreased, and the particles underwent fragmentation.

3. Chipping: As shown in Fig. 8(c), the weathered phyllite grains exhibited multiple cracks with increasing force, which progressively expanded until collapse occurred, resulting in the formation of several minute fragments. The force–displacement curve demonstrated a multipeak pattern, followed by a sharp drop after reaching the highest peak point.

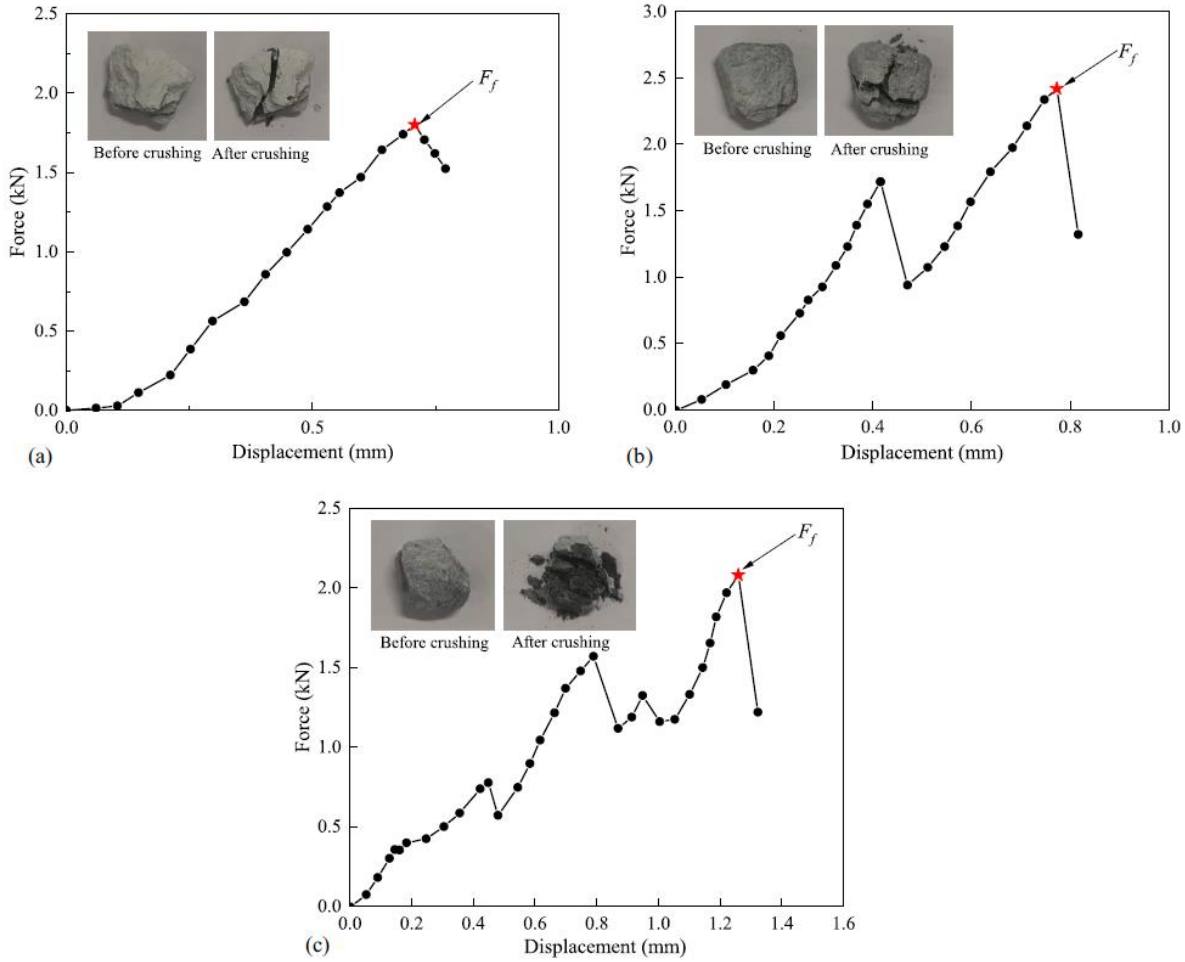

Fig. 8. Fragmentation modes and force–displacement curves of weathered phyllite: (a) fracturing; (b) splitting; and (c) chipping.

Table 3. Statistical results of fragmentation modes

Grain sizes (mm)	Fracturing (%)	Splitting (%)	Chipping (%)
5–10	43	33	24
10–20	52	26	22
20–31.5	58	24	18

Statistical Analysis of Grain Crushing Strength

The crushing strength of a granular material is a crucial characteristic that distinguishes it from other materials. Therefore, studying strength distribution is of great practical importance in engineering. However, accurately determining the crushing strength poses challenges owing to the irregular shape of granular materials (Huang et al. 2020). Currently, researchers widely adopt the characteristic tensile stress to define the grain crushing strength, which is derived from the ratio of the peak loading force to the square of the distance between the upper and lower platens. The following equation has been previously employed by numerous researchers (McDowell and Bolton 1998; Jaeger 1967) to calculate the crushing strength of 300 weathered phyllite grains:

$$\sigma_f = \frac{F_f}{d^2} \tag{1}$$

where σ_f = crushing strength of a single grain; F_f = maximum measured crushing force; and d = diameter of a single grain at failure. For a limited number of grains in the crushing test, the survival probability (P_s) was calculated using the following equation (Nakata et al. 1999):

$$P_s = \frac{N_s(\sigma < \sigma_f)}{N} \tag{2}$$

where N_s = number of particles that are not crushed at the crushing strength σ_f; and N = total number of particles.

Weathered phyllite grains exhibit brittleness, and extensive studies have confirmed the suitability of the Weibull distribution function for describing the strength distribution characteristics of such materials. This has also been validated for other geotechnical granular materials (Huang et al. 2020, 2023; Meng et al. 2022a; Weibull 1951). The occurrence of grain breakage in phyllite is considered a probabilistic event. McDowell and Amon (2000) demonstrated that the survival probability (P_s) of a grain of size d under diametric compression can be determined by

$$p_s(d) = \exp\left[-\left(\frac{d}{d_0}\right)^3\left(\frac{\sigma_f}{\sigma_0}\right)^m\right] \tag{3}$$

where m = Weibull modulus; d_0 = reference size; and σ_0 = characteristic stress for a grain of size d_0 under the assumption that 37% of the tested grains survive.

By substituting $d = d_0$ into Eq. (3), the following linear equation was obtained:

$$\ln[\ln(1/P_s)] = m\ln(\sigma_f) - m\ln(\sigma_0) \tag{4}$$

By plotting $\ln[\ln(1/P_s)]$ against $\ln\sigma_f$, the Weibull modulus (m) can be determined from the slope of the best-fit line using Eq. (4), while σ_0 represents the value of σ_f when $\ln[\ln(1/P_s)] = 0$. Fig. 9 illustrates the test data points and corresponding curves fitted according to Eq. (4).

The strength of the weathered phyllite grains follows a Weibull distribution, which is consistent with the findings reported by Huang et al. (2020) and Oskooei et al. (2021). The Weibull modulus (m) and 37% characteristic strength (σ_0) obtained for the three size groups in this study are as follows: 2.769, 16.89 MPa (5–10 mm); 1.993, 12.7 MPa (10–20 mm); and 1.967, 11.32 MPa (20–31.5 mm). The m value decreased with increasing grain size, indicating an increased dispersion in the crushing strength of the weathered phyllite grains.

Eq. (3) has been successfully applied in analyses of the Weibull modulus for various materials, including carbonate sand (Ma et al. 2019), Quiou sand (McDowell and Bolton 1998), rockfill (Xiao et al. 2019), and railroad ballast (Lim et al. 2004). The characteristic strength of different granular soils adheres to the properties described by the Weibull distribution function. Weibull modulus m represents the variability of the crushing strength distribution: a larger m indicates a more concentrated strength distribution, whereas an increasing particle size corresponds to a decrease in the m value, resulting in a more dispersed strength distribution among the particles.

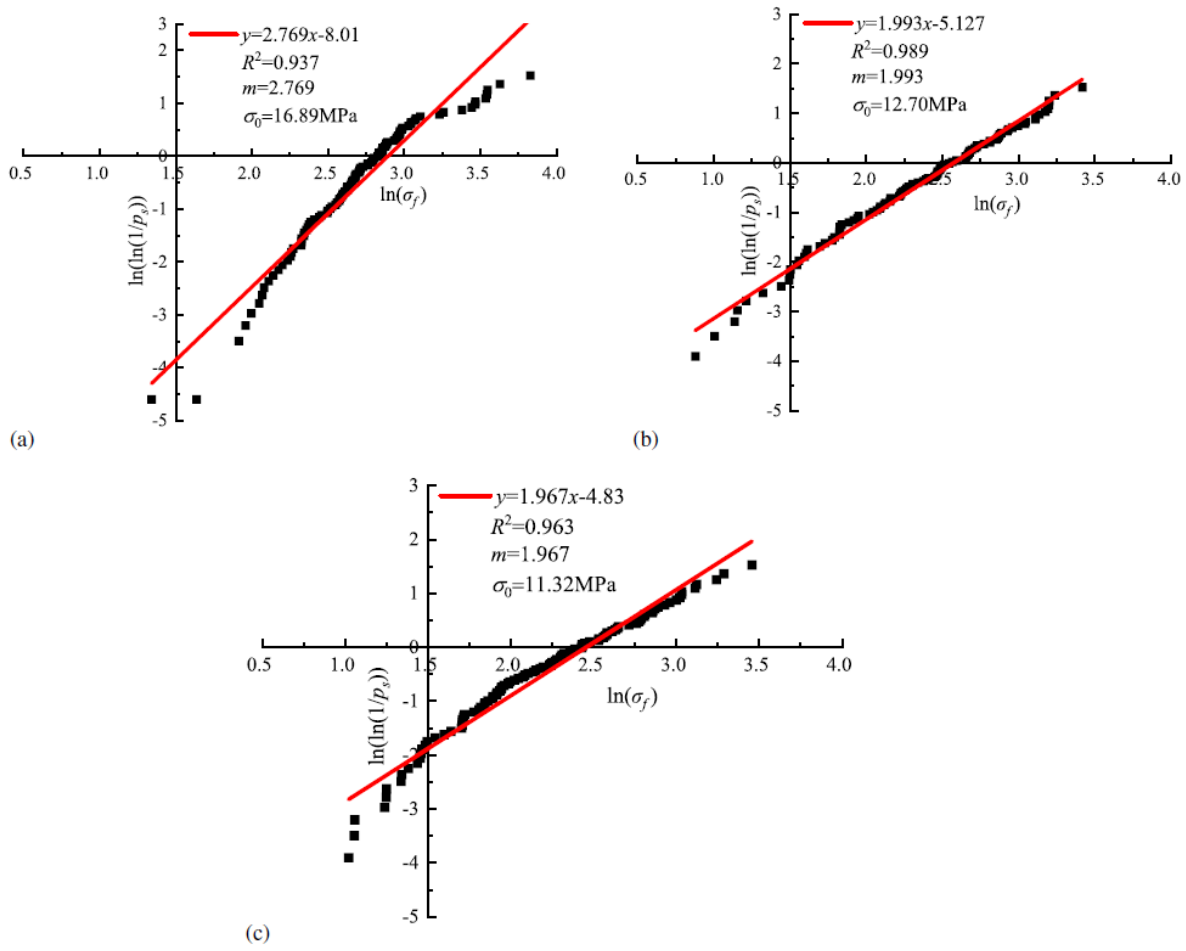

Fig. 9. Weibull survival probability plot for weathered phyllite grain crushing strengths: (a) 5–10 mm; (b) 10–20 mm; and (c) 20–31.5 mm.

Size Effect on Strength Characteristics of Grain Crushing

The strength of geotechnical granular materials exhibits not only discrete behavior but also a significant size effect (Huang et al. 2023; Koutous and Hilali 2019; Kuang et al. 2021; Xiao et al. 2019; Zhao et al. 2021b; Zhou et al. 2013). In this study, the statistical analysis was conducted on the crushing strength (σ_f) and characteristic stress (σ_0) of three different grain-size groups. Fig. 10(a) illustrates the relationship between the crushing strength (σ_f) and the diameter (d) of individual grains at failure, while Fig. 10(b) presents the relationship between the characteristic stress (σ_0) and mean diameter ($\bar{d}$). Based on previous research, it is determined that there is no unique value for the mean diameter ($\bar{d}$). Therefore, we adopted the average value of the actual diameter as the mean diameter ($\bar{d}$) for each size group.

The crushing strength (σ_f) of weathered phyllite grains exhibit a decreasing trend as the grain size increases. Specifically, the average crushing strengths for the three different grain-size groups are 16.01, 11.51, and 10.30 MPa, respectively, indicating a reduction of 5.71 MPa with increasing grain size. Moreover, the characteristic strengths (σ_0) for these three groups with mean diameters ($\bar{d}$) of 6.85, 11.10, and 15.16 mm were determined to be 16.89, 12.70, and 11.32 MPa, respectively, thereby demonstrating a decrease in characteristic stress as the mean diameter increases.

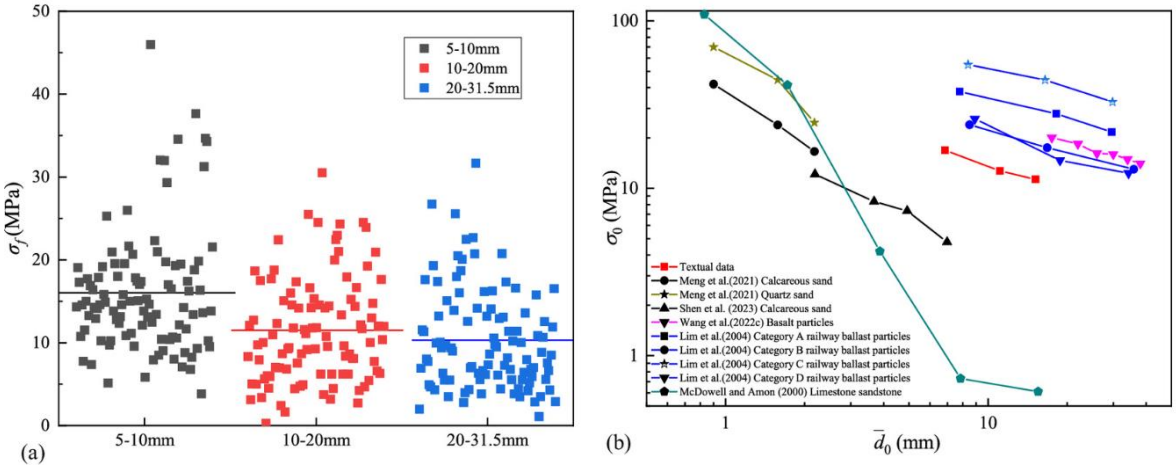

Fig. 10. Crushing strength with particle-size distribution: (a) distribution of the crushing strength with particle diameter; and (b) distribution of the characteristic stress with mean diameter.

The weathered phyllite grains exhibited a pronounced size effect on both the grain crushing strength and characteristic strength. When subjected to the same loading stress, the larger weathered phyllite grains were more prone to fracturing than the smaller grains. This can be attributed to the presence of more cracks and pores within and on the surfaces of larger grains (Marone and Scholz 1989; McDowell and Harireche 2002; Nakata et al. 2001). Under equivalent stress conditions, structural weaknesses increase the likelihood of larger particle failure. In conjunction with previous studies (Lim et al. 2004; McDowell 2002; Wang et al. 2022c), it is evident that the size effect on the characteristic strength of rock grain materials is weaker than that observed for sand and gravel materials (Lim et al. 2004; Meng et al. 2022b; Wang et al. 2022c). As a type of soft rock grain material, weathered phyllite exhibits a similar size effect as rock particle materials, but with less intensity when compared to sand and gravel materials. This discrepancy arises because of the greater prominence of surface roughness and internal defects during the particle size increase in sand and gravel materials.

Grain Shape Effect on Crushing Mode

Studies on grain materials have revealed that the grain shape plays a crucial role in determining their crushing mode (Fu et al. 2017; Kawamoto et al. 2018; Ma et al. 2022; Maroof et al. 2020; Shen et al. 2023; Zhao et al. 2021a). In this study, we selected 100 test particles within the size range of 10–20 mm to investigate the relationship between grain shape and crushing mode. Representative shape parameters, including sphericity, local roundness, and surface roughness, were selected for analysis in each dimension.

The three crushing modes of fracturing, splitting, and chipping accounted for 52%, 26%, and 22%, respectively, in the 10–20-mm size group, with the fracturing mode being predominant. To study the grains in the fracturing mode, four shape parameters including elongation ratio (E_r), flatness ratio (F_r), inscribed circle sphericity (ϕ_0), and convexity (C_X) were selected. For grains in the splitting and chipping modes, two shape parameters including volume sphericity (ϕ_V) and regularity (R) were chosen. The relationship between ϕ_0 and ϕ_V serves as a mutual verification mechanism while that between C_X and R also plays a similar role. This approach ensures accuracy in content analysis.

Frequency distribution histograms and trend lines illustrating the characteristic shape parameters of both the original and broken fragments are shown in Fig. 11. Notably, the frequency of original grains within the gray area ($F_r > 0.495$, $E_r > 0.775$, $\phi_0 > 0.32$, $C_X < 0.03$) in Figs. 11(a–d) is significantly higher compared to that of the broken fragments. Consequently, it can be inferred that weathered phyllite grains exhibit a greater susceptibility to fracturing failure under the following four specific conditions: (1) when their F_r values are smaller, indicating flatter grain shapes; (2) when their E_r values are smaller, suggesting longer particle lengths; (3) when their ϕ_0 values are smaller, implying more pronounced angular characteristics; and (4) when their C_X values are larger, denoting smoother particle surfaces.

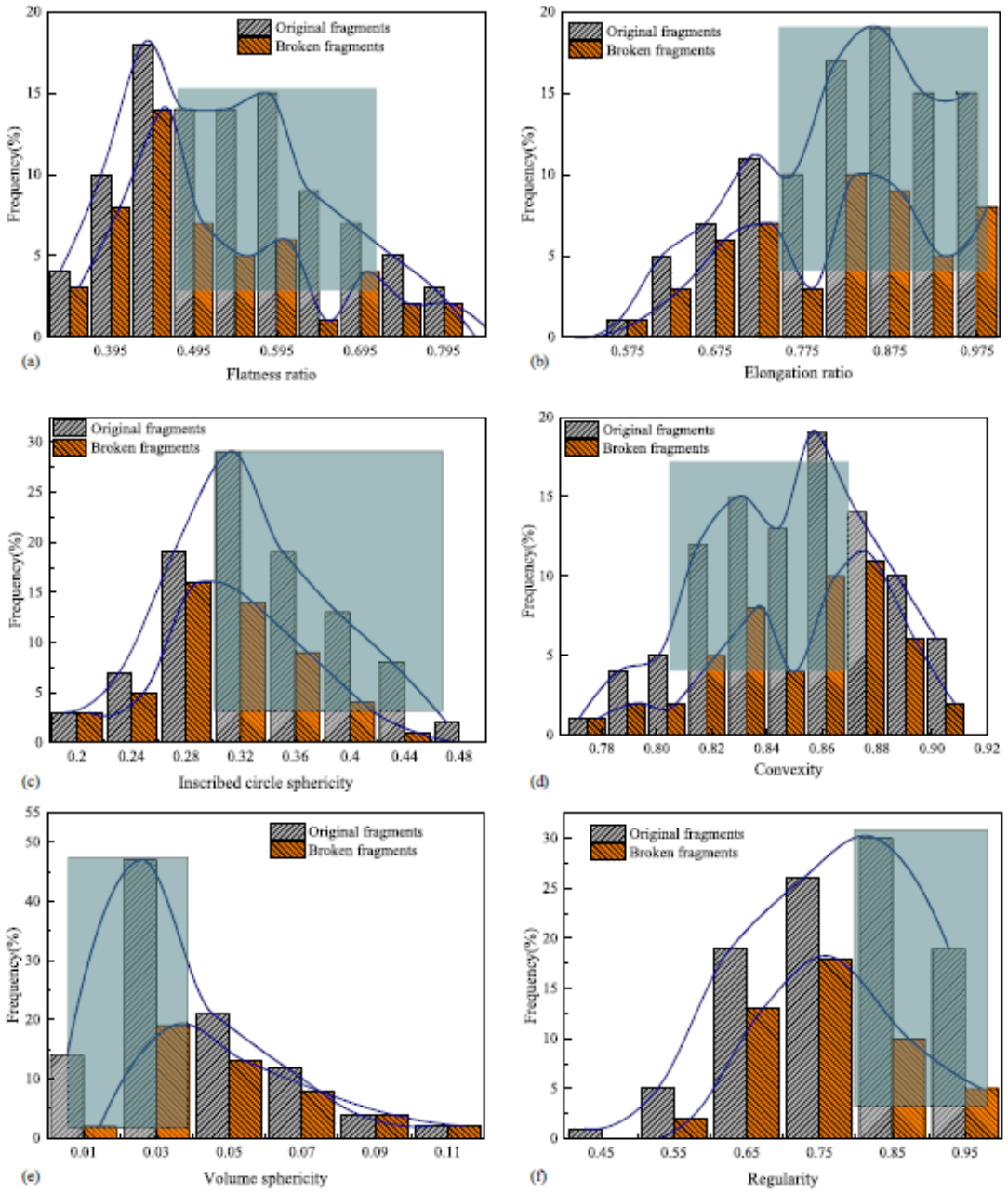

Fig. 11. Frequency distribution histograms of characteristic shape parameters of original and broken fragments: (a) flatness ratio (F_r); (b) elongation ratio (E_r); (c) inscribed circle sphericity (ϕ_0); (d) convexity (C_X); (e) volume sphericity (ϕ_V); and (f) regularity (R).

The frequency of original grains in the dark blue area ($\phi_V < 0.003$, $R > 0.85$) in Figs. 11(e and f) is significantly higher than that of fragmented ones. Hence, it can be inferred that the weathered phyllite grains are more susceptible to splitting and chipping failure under the following two conditions: (1) larger ϕ_V leads to less pronounced angular characteristics of the grains, increasing their likelihood of splitting and chipping, which aligns with the relationship between ϕ_0 and fracturing mode; and (2) smaller R indicates rougher grain surfaces, making them more prone to splitting and chipping failure, consistent with the relationship between C_X and fracturing mode.

Variation of Shape Characteristics before and after Crushing

Grain breakage leads to alterations in the grain size, shape, and other parameters (Daouadji and Hicher 2010). These parameter changes significantly affect the mechanical properties of the grains. Subsequently, 3D scanning was conducted on 300 subgrains ranging from 5 to 31.5 mm formed after the grain crushing test. The shape-characteristic parameters of the subgrains were computed and compared to analyze the variations before and after crushing. This analysis encompassed three dimensions: general form (E_r, F_r, S_f), local roundness (ψ_{3D}, ϕ_0, ϕ_V), and surface roughness (C_X, R).

The variations in the general form parameters before and after crushing are shown in Fig. 12. Following the crushing process, there was a significant increase in the proportion of subgrains with $F_r > 0.55$, leading to a shift in the distribution curve toward $F_r = 1$. Additionally, there was a substantial increase in the proportion of subgrains with $E_r < 0.75$, which resulted in an overall leftward shift in the distribution curve. The mean value of S_f exhibited a slight increasing trend from 3.585 to 3.648 before and after crushing; however, it consistently remained >3, indicating that both the before and after crushing grains maintained their slender shape (Bolton et al. 2008). Consequently, the subgrains predominantly assumed a flat shape, while experiencing reduced elongation and increased slenderness.

The predominant fracturing mode of the grains resulted in halving along a large crack from the middle, leading to significant changes in the long and intermediate axes of the subgrains after crushing. Specifically, the intermediate axis (I) experienced a greater change range than the long axis (L), resulting in a decrease in I/L ratio and an increase in the S/I ratio, ultimately causing the subgrains to become slender, as depicted in Fig. 13.

The local roundness shape parameters before and after grain crushing are shown in Fig. 14. The values of ψ_{3D}, ϕ_0, and ϕ_V decreased following crushing, indicating an enhanced prominence of angular characteristics within the subgrains and a larger deviation from perfect sphericity. After crushing, the overall curve of ψ_{3D} shifted toward the left, accompanied by an increased number of grains with $\psi_{3D} < 0.7$ as well as decreased values for both ϕ_0 and ϕ_V, thus resulting in a more dispersed distribution compared to the precrushing conditions. This can be attributed to the fact that most weathered phyllite particles undergo complete fragmentation during the crushing process, leading to their transformation into irregular fragments and consequently accentuating the subgrain angularity.

The variations in the shape parameters of the surface roughness before and after grain crushing are shown in Fig. 15. Both C_X and R exhibited significant reductions after crushing. There was an increase in the number of grains with $C_X < 0.8$ and $R < 0.85$, leading to a leftward shift in the overall distribution curves. This can be attributed to the pronounced flat characteristics observed

in the weathered phyllite grains. During the single-grain crushing test, the grains were predominantly destroyed perpendicular to the schistosity plane, resulting in uneven fracture surfaces of the subgrains, and consequently, increased surface roughness.

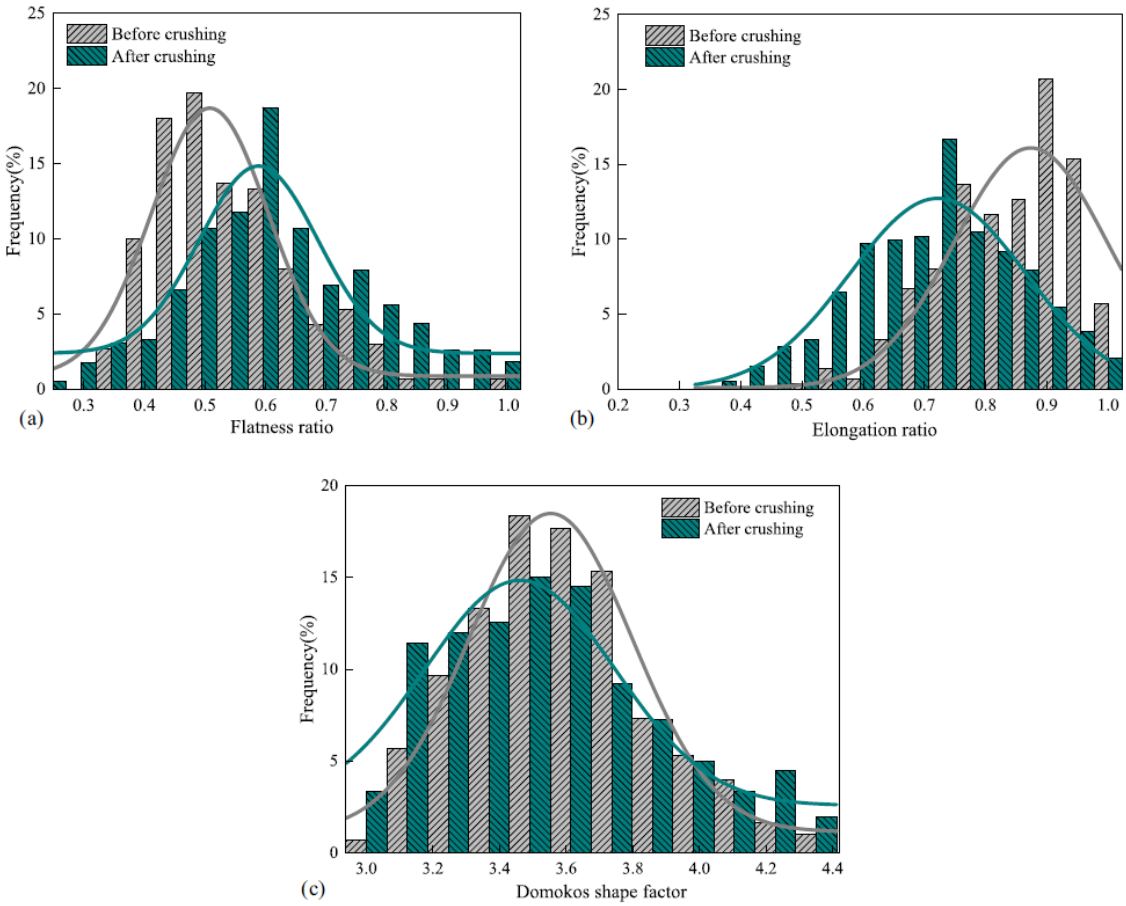

Fig. 12. Frequency distribution histograms of general form parameters before and after crushing: (a) flatness ratio (F_r); (b) elongation ratio (E_r); and (c) Domokos shape factor (S_f).

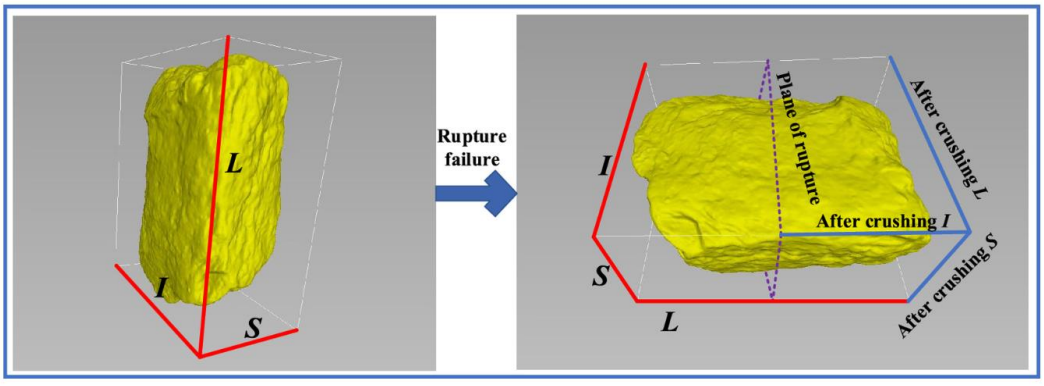

Fig. 13. Schematic diagram of mesoparameter transformation of fracturing mode.

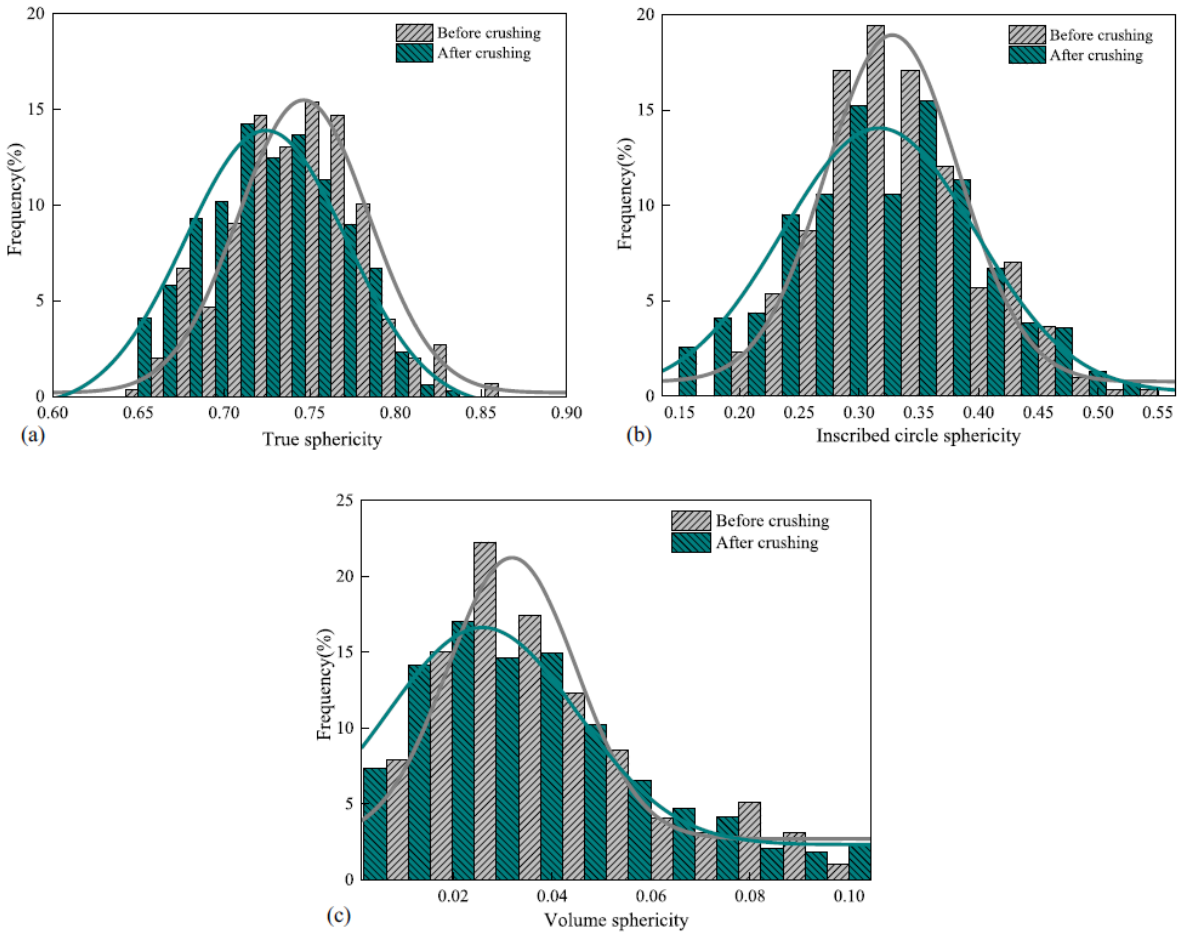

Fig. 14. Frequency distribution histograms of local roundness parameters before and after crushing: (a) true sphericity (ψ_{3D}); (b) inscribed circle sphericity (ϕ_0); and (c) volume sphericity (ϕ_V).

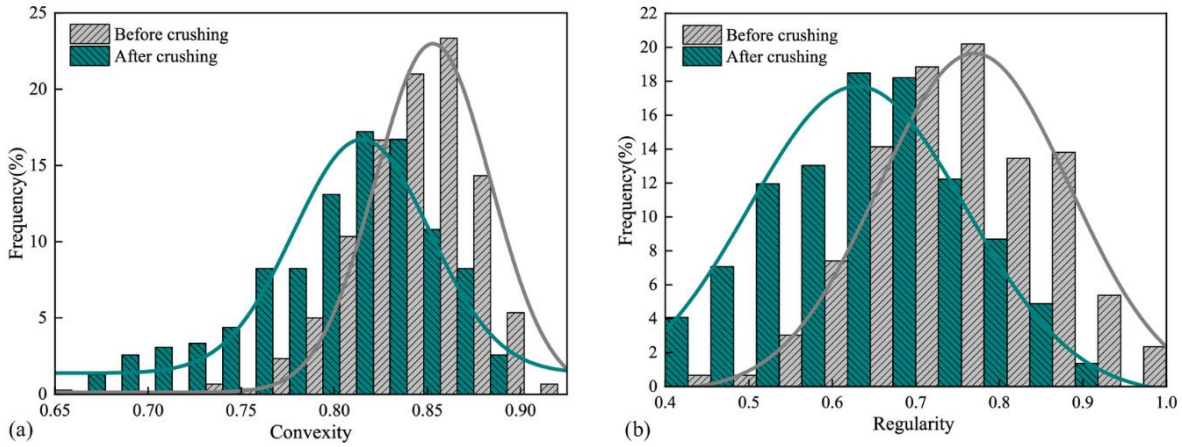

Fig. 15. Frequency distribution histograms of surface roughness parameters before and after crushing: (a) convexity (C_X); and (b) regularity (R).

Conclusion

Single-grain crushing experiments were conducted on weathered phyllite grains of various sizes and shapes, followed by 3D scanning analysis before and after the crushing process. This study investigated the failure load characteristics and effects of crushing mode distribution, crushing strength, size, and grain shape on the grain crushing process, as well as variations in shape characteristics before and after grain fragmentation in weathered phyllite grains. The key findings are summarized as follows:

1. The crushing modes of weathered phyllite grains are categorized based on the grain size into three types: fracturing, splitting, and chipping. The corresponding force–displacement curves exhibited single-peak, double-peak, and multipeak patterns. The occurrence probability of these crushing modes followed the order of fracturing > splitting > chipping. In 300 tests conducted on the weathered phyllite grains, the proportions of the three crushing modes were 51%, 27.7%, and 21.3%, respectively.

2. The crushing strength of the weathered phyllite grains exhibited a satisfactory fit to the Weibull distribution. Specifically, the Weibull moduli for the three size groups (5–10, 10–20, and 20–31.5 mm) were 2.769, 1.993, and 1.967, respectively. Notably, there is an inverse relationship between the grain size and the Weibull modulus, which suggests that the dispersion degree of the crushing strength in weathered phyllite particles increases with larger grain sizes.

3. The crushing process of weathered phyllite grains exhibited a distinct size effect, with the crushing strength showing a tendency to decrease as the grain size increased. The average crushing strengths for the three different size groups were 16.01, 11.51, and 10.30 MPa, respectively. Furthermore, the characteristic strength decreased with an increase in the mean diameter, measuring at 16.89, 12.70, and 11.32 MPa, respectively. As a type of soft rock granular material, weathered phyllite demonstrated a size effect similar to that observed in other rock granular materials but is comparatively weaker than sandstone.

4. The weathered phyllite grains with a flatter and slender morphology displayed more pronounced angularity and smoother particle surfaces, thereby favoring the fracturing mode. Conversely, they are susceptible to splitting and chipping modes. Comparatively, after crushing, the subgrains demonstrated reduced flattening but increased slenderness, angularity, and roughness.

5. Based on the aforementioned observations, it can be stated that most weathered phyllite grains exhibit a flat shape, with some classified as spherical and a small proportion displaying flake and cubic shapes. A smaller flatness ratio, elongation ratio, and inscribed circle sphericity are associated with greater convexity and an increased susceptibility to fracturing failure in weathered phyllite grains. Conversely, higher volume sphericity and lower regularity correlate with a greater tendency for splitting and chipping failures. The crushing strength of the weathered phyllite grains aligns well with the Weibull distribution. Notably, both the Weibull modulus and the dispersion of crushing strength increase with larger grain sizes. The crushing process reveals a distinct size effect, where both crushing strength and characteristic strength tend to decrease as grain size increases. After crushing, the flatness ratio of subgrains increases while the elongation ratio decreases overall; however, the grains maintain an elongated shape. The values of true sphericity, inscribed circle sphericity, and volume sphericity decrease, indicating a heightened angularity within the subgrains. Significant reductions in both convexity and regularity after crushing contribute to uneven fracture surfaces in the subgrains. Therefore, block particles with a high flatness ratio and low elongation ratio are recommended for use as roadbed filler.

References

Bolton, M. D., Y. Nakata, and Y. P. Cheng. 2008. "Micro- and macro-mechanical behaviour of DEM crushable materials." *Géotechnique* 58 (6): 471- 480. https://doi.org/10.1680/geot.2008.58.6.471.

Cignoni, P., M. Callieri, M. Corsini, M. Dellepiane, F. Ganovelli, and G. Ranzuglia. 2008. "Meshlab: An open-source mesh processing tool." In Proc., Eurographics Italian Chapter Conf., 129–136. Salerno, Italy: Eurographics Association.

Daouadji, A., and P.-Y. Hicher. 2010. "An enhanced constitutive model for crushable granular materials." *Int. J. Numer. Anal. Methods Geomech.* 34 (6): 555–580. https://doi.org/10.1002/nag.815.

Deresiewicz, H. 1958. "Mechanics of granular matter." *Adv. Appl. Mech.* 5: 233–306. https://doi.org/10.1016/S0065-2156(08)70021-8.

Domokos, G., F. Kun, A. A. Sipos, and T. Szabo. 2015. "Universality of fragment shapes." *Sci. Rep.* 5: 9147. https://doi.org/10.1038/srep09147.

Feng, L., W. Liu, W. Jiang, and G. Wang. 2024. "Mechanics and road performance of mudstone modified stabilized gravel subgrade in arid desert areas." *Case Stud. Constr. Mater.* 20: e02799. https://doi.org/10.1016/j.cscm.2023.e02799.

Franklin, J. A. 1985. "Suggested method for determining point load strength." *Int. J. Rock Mech. Min. Sci. Geomech. Abstr.* 22 (2): 51–60. https://doi.org/10.1016/0148-9062(85)92327-7.

Fu, R., X. Hu, and B. Zhou. 2017. "Discrete element modeling of crushable sands considering realistic particle shape effect." *Comput. Geotech.* 91: 179–191. https://doi.org/10.1016/j.compgeo.2017.07.016.

Garboczi, E. J., X. Liu, and M. A. Taylor. 2012. "The 3-D shape of blasted and crushed rocks: From 20μm to 38mm." *Powder Technol.* 229: 84–89. https://doi.org/10.1016/j.powtec.2012.06.012.

Garzón, E., M. Cano, B. C. O'Kelly, and P. J. Sánchez-Soto. 2015. "Phyllite clay–cement composites having improved engineering properties and material applications." *Appl. Clay Sci.* 114: 229–233. https://doi.org/10.1016/j.clay.2015.06.006.

Garzón, E., P. J. Sánchez-Soto, and E. Romero. 2010. "Physical and geotechnical properties of clay phyllites." *Appl. Clay Sci.* 48 (3): 307–318. https://doi.org/10.1016/j.clay.2009.12.022.

Hayakawa, Y., and T. Oguchi. 2005. "Evaluation of gravel sphericity and roundness based on surface-area measurement with a laser scanner." *Comput. Geosci.* 31 (6): 735–741. https://doi.org/10.1016/j.cageo.2005.01.004.

Heidari, M., A. A. Momeni, and F. Naseri. 2013. "New weathering classifications for granitic rocks based on geomechanical parameters." *Eng. Geol.* 166 (8): 65–73. https://doi.org/10.1016/j.enggeo.2013.08.007.

Huang, Q., W. Zhou, G. Ma, T.-T. Ng, and K. Xu. 2020. "Experimental and numerical investigation of Weibullian behavior of grain crushing strength." *Geosci. Front.* 11 (2): 401–411. https://doi.org/10.1016/j.gsf.2019.07.007.

Huang, Q., X. Zhou, and B. Liu. 2023. “Effect of realistic shape on grain crushing for rounded and angular granular materials.” *Comput. Geotech.* 162: 105659. https://doi.org/10.1016/j.compgeo.2023.105659.

Illerstrom, A. 1998. “A 3-D laser technique for size, shape and texture analysis of ballast.” *M.S. thesis*. Dept. of Civil and Architectural Engineering, Royal Institute of Technology, Stockholm, Sweden.

Jaeger, J. C. 1967. “Failure of rocks under tensile conditions.” *Int. J. Rock Mech. Min. Sci. Geomech. Abstr.* 4 (2): 219–227. https://doi.org/10.1016/0148-9062(67)90046-0.

Jin, W., X. Yang, F.-c. Yang, and J.-q. Shi. 2024. “Particle breakage of ultra-high dam rockfills under drained shearing.” *Granular Matter* 26: 55. https://doi.org/10.1007/s10035-024-01428-0.

Kashani, H. F., J. P. Hyslip, and C. L. Ho. 2017. “Laboratory evaluation of railroad ballast behavior under heavy axle load and high traffic conditions.” *Transp. Geotech.* 11: 69–81. https://doi.org/10.1016/j.trgeo.2017.04.002.

Kawamoto, R., J. Andrade, and T. Matsushima. 2018. “A 3-D mechanics-based particle shape index for granular materials.” *Mech. Res. Commun.* 92: 67–73. https://doi.org/10.1016/j.mechrescom.2018.07.002.

Koutous, A., and E. Hilali. 2019. “Grain shape effects on the mechanical behavior of compacted earth.” *Case Stud. Constr. Mater.* 11: e00303. https://doi.org/10.1016/j.cscm.2019.e00303.

Kuang, D., Z. Long, R. Guo, and P. Yu. 2021. “Experimental and numerical investigation on size effect on crushing behaviors of single calcareous sand particles.” *Mar. Georesour. Geotechnol.* 39 (5): 543–553. https://doi.org/10.1080/1064119X.2020.1725194.

Lanaro, F., and P. Tolppanen. 2002. “3D characterization of coarse aggregates.” *Eng. Geol.* 65 (1): 17–30. https://doi.org/10.1016/S0013-7952(01)00133-8.

Latham, J. P., A. Munjiza, X. Garcia, J. Xiang, and R. Guises. 2008. “Three-dimensional particle shape acquisition and use of shape library for DEM and FEM/DEM simulation.” *Miner. Eng.* 21 (11): 797–805. https://doi.org/10.1016/j.mineng.2008.05.015.

Le, Z., Q. Yu, W. Zhu, H. Liu, and T. Yang. 2021. “Experimental study on the effect of granular backfill with various gradations on the mechanical behavior of rock.” *Int. J. Min. Sci. Technol.* 31 (5): 889–899. https://doi.org/10.1016/j.ijmst.2021.07.001.

Li, J., Y. Huang, Z. Chen, J. Zhang, H. Jiang, and Y. Zhang. 2019. “Characterizations of macroscopic deformation and particle crushing of crushed gangue particle material under cyclic loading: In solid backfilling coal mining.” *Powder Technol.* 343: 159–169. https://doi.org/10.1016/j.powtec.2018.11.049.

Li, X., Y. Lv, Y. Su, K. Zou, Y. Wang, and W. Huang. 2023. “Coupling effects of morphology and inner pore distribution on the mechanical response of calcareous sand particles.” *J. Rock Mech. Geotech. Eng.* 15 (6): 1565–1579. https://doi.org/10.1016/j.jrmge.2022.09.017.

Li, Y., Y. Zhang, J. Bi, Y. Zhao, Y. Li, X. Zhong, and K. Zheng. 2024. “Influences of calcium and magnesium sources on microbially modified strongly weathered phyllite filler.” *Constr. Build. Mater.* 416: 135118. https://doi.org/10.1016/j.conbuildmat.2024.135118.

Liang, H., Y. Shen, J. Xu, and S. Chen. 2022. "Multiscale morphological effects on stress-dilation behaviors of natural sands: A 3D printing simulation method." *J. Eng. Mech.* 148 (9): 04022046. https://doi.org/10.1061/(ASCE)EM.1943-7889.0002128.

Lim, W. L., G. R. McDowell, and A. C. Collop. 2004. "The application of Weibull statistics to the strength of railway ballast." *Granular Matter* 6: 229–237. https://doi.org/10.1007/s10035-004-0180-z.

Liu, F., X. Mao, Y. Fan, L. Wu, and W. V. Liu. 2020. "Effects of initial particle gradation and rock content on crushing behaviors of weathered phyllite fills—A case of eastern Ankang section of Shiyan–Tianshui highway, China." *J. Rock Mech. Geotech. Eng.* 12 (2): 269–278. https://doi.org/10.1016/j.jrmge.2019.07.011.

Ma, G., Y. Wang, H. Zhou, X. Lu, and W. Zhou. 2022. "Morphology characteristics of the fragments produced by rock grain crushing." *Int. J. Geomech.* 22 (4): 04022020. https://doi.org/10.1061/(ASCE)GM.1943-5622.0002329.

Ma, G., W. Zhou, R. A. Regueiro, Q. Wang, and X. Chang. 2017. "Modeling the fragmentation of rock grains using computed tomography and combined FDEM." *Powder Technol.* 308: 388–397. https://doi.org/10.1016/j.powtec.2016.11.046.

Ma, G., W. Zhou, Y. Zhang, Q. Wang, and X. Chang. 2018. "Fractal behavior and shape characteristics of fragments produced by the impact of quasi-brittle spheres." *Powder Technol.* 325: 498–509. https://doi.org/10.1016/j.powtec.2017.11.030.

Ma, L., Z. Li, M. Wang, H. Wei, and P. Fan. 2019. "Effects of size and loading rate on the mechanical properties of single coral particles." *Powder Technol.* 342: 961–971. https://doi.org/10.1016/j.powtec.2018.10.037.

Maerz, N. H., and M. Luscher. 2001. "Measurement of flat and elongation of coarse aggregate using digital image processing." *Transportation Research Board, 80th Annual Meeting, Washington, DC*.

Mao, X. S., C. J. Miller, and L. Q. Liu. 2017. "Cement improved highly weathered phyllite for highway roadbeds: A case study in Shaanxi province." *J. Traffic Transp. Eng.* 4 (4): 403–411. https://doi.org/10.1016/j.jtte.2017.07.003.

Marachi, N. 1969. *Strength and deformation characteristics of rockfill materials*. Berkeley, CA: Univ. of California.

Marone, C., and C. H. Scholz. 1989. "Particle-size distribution and microstructures within simulated fault gouge." *J. Struct. Geol.* 11 (7): 799–814. https://doi.org/10.1016/0191-8141(89)90099-0.

Maroof, M. A., A. Mahboubi, A. Noorzad, and Y. Safi. 2020. "A new approach to particle shape classification of granular materials." *Transp. Geotech.* 22: 100296. https://doi.org/10.1016/j.trgeo.2019.100296.

McDowell, G. R. 2002. "On the yielding and plastic compression of sand." *Soils Found.* 42 (1): 139–145. https://doi.org/10.3208/sandf.42.1139.

McDowell, G. R., and A. Amon. 2000. "The application of Weibull statistics to the fracture of soil particles." *Soils Found.* 40 (5): 133–141. https://doi.org/10.3208/sandf.40.5_133.

McDowell, G. R., and M. D. Bolton. 1998. “On the micromechanics of crushable aggregates.” *Géotechnique* 48 (5): 667–679. https://doi.org/10.1680/geot.1998.48.5.667.

McDowell, G. R., and O. Harireche. 2002. “Discrete element modelling of soil particle fracture.” *Géotechnique* 52 (5): 131–135. https://doi.org/10.1680/geot.2002.52.2.131.

McKenna, G., S. A. Argyroudis, M. G. Winter, and S. A. Mitoulis. 2021. “Multiple hazard fragility analysis for granular highway embankments: Moisture ingress and scour.” *Transp. Geotech.* 26: 100431. https://doi.org/10.1016/j.trgeo.2020.100431.

Meng, M., Y. Xiao, X. Duan, Z. Sun, L. Du, H. Fan, and H. Liu. 2022a. “Crushing strength of artificial single-particle considering the effect of particle morphology.” *Acta Geotech.* 17 (9): 3909–3926. https://doi.org/10.1007/s11440-022-01516-6.

Meng, M. Q., Z. X. Yuan, and X. Jiang. 2022b. “Experimental study of the single-particle crushing-strength-size effect of calcareous sand–quartz sand.” *Sci. Sin. Technol.* 52: 1035–1047. https://doi.org/10.1360/SST-2021-0241.

Miščević, P., and G. Vlastelica. 2019. “Estimation of embankment settlement caused by deterioration of soft rock grains.” *Bull. Eng. Geol. Environ.* 78: 1843–1853. https://doi.org/10.1007/s10064-017-1203-4.

Mollon, G., and J. Zhao. 2012. “Fourier-Voronoi-based generation of realistic samples for discrete modelling of granular materials.” *Granular Matter* 14: 621–638. https://doi.org/10.1007/s10035-012-0356-x.

Nakata, Y., A. F. L. Hyde, M. Hyodo, and H. Murata. 1999. “A probabilistic approach to sand particle crushing in the triaxial test.” *Géotechnique* 49 (5): 567–583. https://doi.org/10.1680/geot.1999.49.5.567.

Nakata, Y., M. Hyodo, A. F. L. Hyde, Y. Kato, and H. Murata. 2001. “Microscopic particle crushing of sand subjected to high pressure one-dimensional compression.” *Soils Found.* 41 (1): 69–82. https://doi.org/10.3208/sandf.41.69.

Necochea, J. E., E. Sáez, and K. J. Hanley. 2024. “Effect of sand particle shape on micromechanical modeling in direct shear testing.” *Comput. Geotech.* 169: 106222. https://doi.org/10.1016/j.compgeo.2024.106222.

Neveu, A., R. Artoni, P. Richard, and Y. Descantes. 2016. “Fracture of granular materials composed of arbitrary grain shapes: A new cohesive interaction model.” *J. Mech. Phys. Solids* 95: 308–319. https://doi.org/10.1016/j.jmps.2016.06.008.

Oskooei, P. R., A. Mohammadinia, A. Arulrajah, and S. Horpibulsuk. 2021. “DEM modeling and experimental analysis of the breakage behavior of recycled crushed brick particles.” *Transp. Geotech.* 30: 100586. https://doi.org/10.1016/j.trgeo.2021.100586.

Ouhbi, N., C. Voivret, G. Perrin, and J.-N. Roux. 2017. “3D particle shape modelling and optimization through proper orthogonal decomposition.” *Granular Matter* 19: 86. https://doi.org/10.1007/s10035-017-0771-0.

Pouranian, M. R., M. Shishehbor, and J. E. Haddock. 2020. “Impact of the coarse aggregate shape parameters on compaction characteristics of asphalt mixtures.” *Powder Technol.* 363: 369–386. https://doi.org/10.1016/j.powtec.2020.01.014.

Riviera, P. P., R. Bellopede, P. Marini, and M. Bassani. 2014. "Performance-based re-use of tunnel muck as granular material for subgrade and sub-base formation in road construction." *Tunnelling Underground Space Technol.* 40: 160–173. https://doi.org/10.1016/j.tust.2013.10.002.

Sefi, F., and M. A. Lav. 2022. "Evaluation of a new grain breakage factor based on the single grain crushing strength." *Transp. Geotech.* 33: 100733. https://doi.org/10.1016/j.trgeo.2022.100733.

Shen, J., H. Wang, B. Zhou, G. Hu, X. Zhang, and B. Yang. 2023. "Investigation of the effect of microbial-induced calcite precipitation treatment on bio-cemented calcareous sands using discrete element method." *Comput. Geotech.* 158: 105365. https://doi.org/10.1016/j.compgeo.2023.105365.

Shi, X. S., K. Liu, and J. Yin. 2021. "Effect of initial density, particle shape, and confining stress on the critical state behavior of weathered gap-graded granular soils." *J. Geotech. Geoenviron. Eng.* 147 (2): 04020160. https://doi.org/10.1061/(ASCE)GT.1943-5606.0002449.

Singh, T. N., A. Kainthola, and A. Venkatesh. 2012. "Correlation between point load index and uniaxial compressive strength for different rock types." *Rock Mech. Rock Eng.* 45: 259–264. https://doi.org/10.1007/s00603-011-0192-z.

Sun, Y., B. Indraratna, and S. Nimbalkar. 2014. "Three-dimensional characterisation of particle size and shape for ballast." *Géotechnique Lett.* 4 (3): 197–202. https://doi.org/10.1680/geolett.14.00036.

Wang, B., U. Martin, and S. Rapp. 2017. "Discrete element modeling of the single-particle crushing test for ballast stones." *Comput. Geotech.* 88: 61–73. https://doi.org/10.1016/j.compgeo.2017.03.007.

Wang, H., R. Zentar, and D. Wang. 2022a. "Rheological characterization of fine-grained sediments under steady and dynamic conditions." *Int. J. Geomech.* 22 (1): 04021260. https://doi.org/10.1061/(ASCE)GM.1943-5622.0002243.

Wang, H., R. Zentar, D. Wang, L. Dong, and D. Sun. 2024. "Recycling single use surgical face mask waste for reinforcing cement-treated/untreated dredged marine sediments: Strength, deformation and micro-mechanisms analysis." *Constr. Build. Mater.* 449: 138450. https://doi.org/10.1016/j.conbuildmat.2024.138450.

Wang, H., R. Zentar, D. Wang, and F. Ouendi. 2022b. "New applications of ordinary Portland and calcium sulfoaluminate composite binder for recycling dredged marine sediments as road materials." *Int. J. Geomech.* 22 (6): 04022068. https://doi.org/10.1061/(ASCE)GM.1943-5622.0002373.

Wang, J., S. Chi, X. Shao, and X. Zhou. 2022c. "Representative elementary volume analysis of EB constitutive model parameters of rockfill materials using DEM." *Powder Technol.* 406: 117569. https://doi.org/10.1016/j.powtec.2022.117569.

Wang, W., and M. R. Coop. 2016. "An investigation of breakage behaviour of single sand particles using a high-speed microscope camera." *Géotechnique* 66 (12): 984–998. https://doi.org/10.1680/jgeot.15.P.247.

Wei, Z., C. Xiaolin, Z. Chuangbing, and L. Xinghong. 2010. "Creep analysis of high concrete-faced rockfill dam." *Int. J. Numer. Methods Biomed. Eng.* 26 (11): 1477–1492. https://doi.org/10.1002/cnm.1230.

Weibull, W. 1951. “A statistical distribution function of wide applicability.” *J. Appl. Mech.* 18: 293–297. https://doi.org/10.1115/1.4010337.

Wen, P., C. Wang, L. Song, H. Chen, and M. Chen. 2025. “A comprehensive evaluation on particles breakage characteristics of waste *Argillaceous gangue* as subgrade filler.” *Road Mater. Pavement Des.* 26 (3): 477–496. https://doi.org/10.1080/14680629.2024.2

Werkmeister, S., A. R. Dawson, and F. Wellner. 2005. “Permanent deformation behaviour of granular materials.” *Road Mater. Pavement Des.* 6 (1): 31–51. https://doi.org/10.1080/14680629.2005.9689998.

Wu, J. Y. 2004. “The settlement behaviors of granular backfill materials for high speed rail embankment.” *ASCE Geotech. Spec. Publ.* 2 (126): 1584–1591. https://doi.org/10.1061/40744(154)150.

Wu, M., and J. Wang. 2024. “Exploring particle breakage in sand under triaxial shearing using combined X-ray tomography and particle tracking method.” *Géotechnique* 74: 1684–1699. https://doi.org/10.1680/jgeot.22.00351.

Xiao, Y., C. S. Desai, A. Daouadji, A. W. Stuedlein, H. Liu, and H. Abuel-Naga. 2020a. “Grain crushing in geoscience materials—Key issues on crushing response, measurement and modeling: Review and preface.” *Geosci. Front.* 11 (2): 363–374. https://doi.org/10.1016/j.gsf.2019.11.006.

Xiao, Y., L. Long, T. M. Evans, H. Zhou, H. Liu, and A. W. Stuedlein. 2019. “Effect of particle shape on stress-dilatancy responses of medium-dense sands.” *J. Geotech. Geoenviron. Eng.* 145 (2): 04018105. https://doi.org/10.1061/(ASCE)GT.1943-5606.0001994.

Xiao, Y., M. Meng, A. Daouadji, Q. Chen, Z. Wu, and X. Jiang. 2020b. “Effects of particle size on crushing and deformation behaviors of rockfill materials.” *Geosci. Front.* 11 (2): 375–388. https://doi.org/10.1016/j.gsf.2018.10.010.

Xie, W.-Q., X.-P. Zhang, X.-M. Yang, Q.-S. Liu, S.-H. Tang, and X.-B. Tu. 2020. “3D size and shape characterization of natural sand particles using 2D image analysis.” *Eng. Geol.* 279: 105915. https://doi.org/10.1016/j.enggeo.2020.105915.

Yin, S., Z. Guo, Q. Wang, Y. Zhao, and Y. Li. 2023. “Effects of particle size on compressive deformation characteristics of broken rock mass in gangue rib of automatically formed gob-side entry retaining.” *Powder Technol.* 430: 118987. https://doi.org/10.1016/j.powtec.2023.118987.

Ying, M., F. Liu, J. Wang, C. Wang, and M. Li. 2021. “Coupling effects of particle shape and cyclic shear history on shear properties of coarse-grained soil-geogrid interface.” *Transp. Geotech.* 27: 100504. https://doi.org/10.1016/j.trgeo.2020.100504.

Zhang, Y. J., X. Wang, Y. X. Yin, and L. Zhao. 2014. “Experimental study on railway subgrade filling material of phyllite spoil improved with cement.” *J. China Railway Soc.* 36 (6): 81–86. https://doi.org/10.3969/j.issn.1001-8360.2014.06.013.

Zhao, L., S. Zhang, M. Deng, and X. Wang. 2021a. “Statistical analysis and comparative study of multi-scale 2D and 3D shape features for unbound granular geomaterials.” *Transp. Geotech.* 26: 100377. https://doi.org/10.1016/j.trgeo.2020.100377.

Zhao, X., D. Elsworth, Y. He, W. Hu, and T. Wang. 2021b. “A grain texture model to investigate effects of grain shape and orientation on macro-mechanical behavior of crystalline rock.” *Int. J. Rock Mech. Min. Sci.* 148: 104971. https://doi.org/10.1016/j.ijrmms.2021.104971.

Zhao, X., Z. Fu, Q. Yang, K. Yao, D. Geng, and K. Li. 2021c. "Subgrade fill strength and bearing characteristics of weathered phyllite blended with red clay." *Road Mater. Pavement Des.* 22 (11): 2571–2590. https://doi.org/10.1080/14680629.2020.1773906.

Zheng, J., and R. D. Hryciw. 2015. "Traditional soil particle sphericity, roundness and surface roughness by computational geometry." *Géotechnique* 65 (6): 494–506. https://doi.org/10.1680/geot.14.P.192.

Zheng, J., and R. D. Hryciw. 2017. "Soil particle size and shape distributions by stereophotography and image analysis." *Geotech. Test. J.* 40 (2): 317–328. https://doi.org/10.1520/GTJ20160165.

Zheng, S.-F., Y. Liu, N. Zhang, X. Li, and L. Gao. 2022. "Experimental studies on shape and size effects on particle breakage of railway ballast." *Transp. Geotech.* 37: 100883. https://doi.org/10.1016/j.trgeo.2022.100883.

Zheng, W., X. Hu, and D. D. Tannant. 2020. "Shape characterization of fragmented sand grains via X-ray computed tomography imaging." *Int. J. Geomech.* 20 (3): 04020003. https://doi.org/10.1061/(ASCE)GM.1943-5622.0001599.

Zheng, W., X. Hu, D. D. Tannant, K. Zhang, and C. Xu. 2019. "Characterization of two- and three-dimensional morphological properties of fragmented sand grains." *Eng. Geol.* 263: 105358. https://doi.org/10.1016/j.enggeo.2019.105358.

Zhou, B., D. Wei, Q. Ku, J. Wang, and A. Zhang. 2020. "Study on the effect of particle morphology on single particle breakage using a combined finite-discrete element method." *Comput. Geotech.* 122: 103532. https://doi.org/10.1016/j.compgeo.2020.103532.

Zhou, W., G. Ma, X. Chang, and C. Zhou. 2013. "Influence of particle shape on behavior of rockfill using a three-dimensional deformable DEM." *J. Eng. Mech.* 139: 1868–1873. https://doi.org/10.1061/(ASCE)EM.1943-7889.0000604.

Zhou, X., G. Ma, and Y. Zhang. 2019. "Grain size and time effect on the deformation of rockfill dams: A case study on the Shuibuya CFRD." *Géotechnique* 69 (7): 606–619. https://doi.org/10.1680/jgeot.17.P.299.

Zingg, T. 1935. "Beitrag zur Schotteranalyse." *Schweiz. Mineral. Petrogr. Mitt.* 15: 39–140.